REFERENCES

1. S. W. Yuan and A. B. Finkelstein, Heat transfer in laminar pipe flow with uniform coolant injection, *Jet Propulsion* **28**, 178–181 (1958).
2. R. M. Terrill, Heat transfer in laminar flow between parallel porous plates, *Int. J. Heat Mass Transfer* **8**, 1491–1497 (1965).
3. W. M. Kays and H. C. Perkins, Forced convection, internal flow in ducts, in *Handbook of Heat Transfer Fundamentals*, 2nd Edn (Edited by W. M. Rohsenow, J. P. Hartnett and E. N. Gario). McGraw-Hill, New York (1985).
4. G. J. Hwang, Y. C. Cheng and M. L. Ng, Developing laminar flow and heat transfer in a square duct with one-walled injection and suction, *Int. J. Heat Mass Transfer* **36**, 2429–2440 (1993).
5. G. J. Hwang, Y. C. Cheng and M. L. Ng, Friction factors and heat transfer correlations for gaseous reactant flow in fuel cell power modules. In: *Proceedings of the 6th Int. Symp. on Transport Phenomena in Thermal Engineering*, Vol. 1, pp. 685–690 (1993).
6. Y. C. Cheng and G. J. Hwang, Experimental studies of laminar flow and heat transfer in a one-porous-wall square duct with injection flow, *Int. J. Heat Mass Transfer* **38**, 3475–3484 (1995).
7. C. J. Hsu, An exact analysis of low Peclet number thermal entry heat transfer in transversely nonuniform velocity fields, *AIChE J.* **17**, 732–740 (1971).

Pergamon

Int. J. Heat Mass Transfer. Vol. 40, No. 2, pp. 485–490, 1997

0017–9310/97 $15.00+0.00

PII: 50017–9300(96)00105–6

Natural convection in porous media near L-shaped corners

I. POP
Faculty of Mathematics, University of Cluj, R-3400 Cluj, CP253, Romania

and

D. ANGIRASA and G. P. PETERSON†
Department of Mechanical Engineering, Texas A & M University, College Station, TX 77843-3123, U.S.A.

(*Received* 30 *August* 1995 *and in final form* 15 *March* 1996)

1. INTRODUCTION

Natural convection in porous media has applications such as building insulation, underground energy and geophysical systems. Since the similarity analysis of Cheng and Minkowycz [1] on natural convection from a vertical surface, numerous studies have been reported in the literature [2]. However, natural convection heat transfer from L-shaped corners in porous media, which has geophysical and technological applications has received much less attention.

Daniels and Simpkins [3] studied natural convection in the region bounded by a uniformly heated vertical wall and a thermally insulated wall which forms a corner of arbitrary angle. Hsu and Cheng [4] considered a semi-infinite inclined heated surface, attached to another unheated surface extending upstream at an arbitrary angle. In both of these investigations [3,4], the method of matched asymptotic expansions was used. Related problems of natural convection from vertical corners placed in a porous medium have also been investigated [5–7].

In the current work, numerical solutions for natural convection in a Darcian fluid confined in the region of a horizontal, L-shaped corner are presented. The corner is formed by a heated isothermal vertical plate joined to a horizontal surface, which is either adiabatic, or held at ambient temperature. The aspect ratio range considered (i.e. the length of the horizontal side/height of the vertical side) falls between the two asymptotic limits of no horizontal wall, and a 'long' wall.

2. ANALYSIS

Steady, two-dimensional (2D) natural convection of a Darcian fluid from an L-shaped corner is considered as shown in Fig. 1, where the coordinate system and the boundary conditions in non-dimensional form are marked. The saturated porous medium is treated as a continuum, with the solid and fluid phases in local thermodynamic equilibrium. The governing equations can be reduced to the following coupled differential equations for the velocity components and temperature in nondimensional form

† Author to whom correspondence should be addressed.

NOMENCLATURE

g	gravitational acceleration
K	permeability
L	height of the vertical surface
Nu	average Nusselt number for the vertical surface of a corner [equation (6)]
Nu_0	average Nusselt number for a lone vertical surface
Ra	Rayleigh number, $g\beta K(t_w-t_\infty)L/\nu\alpha$
t	temperature
T	non-dimensional temperature [equation (4)]
u, v	velocity components in x and y-directions, respectively
U, V	non-dimensional velocity components
U_c	reference velocity, $g\beta K(t_w-t_\infty)/\nu$
W	length of the horizontal surface
W^*	non-dimensional length of the horizontal surface $= W/L$
x, y	space coordinates in vertical and horizontal directions, respectively
X, Y	non-dimensional space coordinates [equation (4)].

Greek symbols

α	thermal diffusivity
β	coefficient of thermal expansion
ν	kinematic viscosity
σ	ratio of heat capacities of the saturated porous medium and the fluid
τ	time
τ^*	non-dimensional time [equation (4)]
ψ	streamfunction
ω	vorticity.

Subscripts

w	wall
∞	location far away from the wall.

$$\frac{\partial U}{\partial X}+\frac{\partial V}{\partial Y}=0 \tag{1}$$

$$\frac{\partial U}{\partial Y}-\frac{\partial V}{\partial X}=\frac{\partial T}{\partial Y} \tag{2}$$

$$\frac{\partial T}{\partial \tau^*}+U\frac{\partial T}{\partial X}+V\frac{\partial T}{\partial Y}=\frac{1}{Ra}\left(\frac{\partial^2 T}{\partial X^2}+\frac{\partial^2 T}{\partial Y^2}\right) \tag{3}$$

where $Ra=g\beta K(t_w-t_\infty)L/\alpha\nu$ is the modified Rayleigh number for the porous medium. In arriving at the equations (1)–(3), the following non-dimensional variables were defined.

$$X=x/L \quad Y=y/L \quad \tau^*=\frac{\tau U_c}{L\sigma} \quad U=u/U_c$$

$$V=v/U_c \quad \text{and} \quad T=\frac{t-t_\infty}{t_w-t_\infty} \tag{4}$$

where σ is the ratio of heat capacities of the stagnant medium and the fluid. The reference convective velocity U_c is given by $g\beta K(t_w-t_\infty)/\nu$, where α and ν are the thermal diffusivity and the kinematic viscosity, respectively.

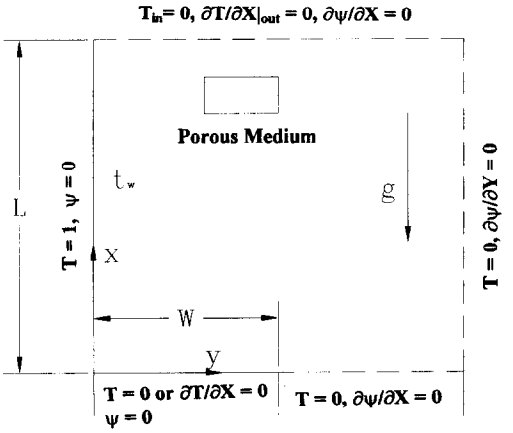

Fig. 1. The physical configuration and the numerical boundary conditions.

By defining vorticity, ω, as

$$\left(\frac{\partial U}{\partial Y}-\frac{\partial V}{\partial X}\right),$$

equation (2) can be expressed as

$$\omega=\frac{\partial T}{\partial Y},$$

and a stream function, ψ, can be defined such that

$$U=\frac{\partial \psi}{\partial Y}, \quad \text{and} \quad V=-\frac{\partial \psi}{\partial X}.$$

With this formulation, it follows that

$$\nabla^2\psi=\omega. \tag{5}$$

The average Nusselt number for the vertical heated surface of the L-shaped corner with the horizontal side either adiabatic or isothermal at the ambient temperature is expressed as

$$\overline{Nu}=\int_0^1\left(-\frac{\partial T}{\partial Y}\right)_{Y=0}\mathrm{d}X. \tag{6}$$

3. NUMERICAL PROCEDURES

The non-dimensional variables for which a solution is sought are the temperature, T, and the streamfunction, ψ. For this, the energy equation, equation (3) and the streamfunction equation (5) are numerically solved with standard ADI-SOR methods [9]. The vorticity and the velocity components are then evaluated using the definitions given above. For the energy equation, upwind differencing is used for the convective terms and the central-difference formulation for the diffusion terms. Both the absolute and relative error criteria are employed to check for steady-state (temperature) and for iterative convergence (streamfunction). The non-dimensional time-step for the marching of the energy equation (3) is 0.001 and uniform grid-spacings are employed in each direction. The average Nusselt number, Nu, is obtained by numerically integrating equation (6) using Simpson's rule. To consider the uncertainties of the end-points, an open-ended formula is employed [10].

Following ref. [8], the computational domain can be deter-

mined as follows. For $W^* \geq 2\delta^*_L$, where $\delta^*_L (= \delta/L)$ is the non-dimensional boundary layer thickness adjacent to the vertical surface at $X = 1$, the computational domain is formed as a rectangle with sides of $X_{max} = 1$ and $Y_{max} = W^*$. For $W^* < 2\delta^*$, $Y_{max} = 2\delta^*$ forms the horizontal side of the calculation domain. For further discussion on the rationale behind this choice, see ref. [8].

The boundary layer thickness on the vertical leg of the corner is dependent upon the Rayleigh number, Ra, and may be estimated from the analysis of Cheng and Minkowycz [1]. This is given by $\delta/x = 6.31/\sqrt{Ra_x}$ and hence it follows that $\delta_L^* = 6.31/\sqrt{Ra}$.

The solution of equations (3) and (5) requires boundary conditions only for T and ψ. These are shown in Fig. 1. The initial conditions for marching the discretized energy equation (3) are $\tau^* = 0$: $U = 0$, $V = 0$ and $T = 0$ for all X and Y.

The accuracy of the numerical solution depends on the resolution of the flow and temperature fields in the vertical boundary layer. Hence, a series of calculations was first performed for $W^* = 0$ and a high Rayleigh number, $Ra = 10^3$, by varying the number of grid-points in each direction. In the results that follow, the number of grid-points chosen for $W^* = 0$ is 101×101 and for the L-shaped corner is 51×151. The temperature and velocity gradients near the wall are less steep for the corner flow than for the lone vertical surface. With this grid size, the numerical errors are estimated to be less than 1% in the field variables and 2% in the Nusselt number.

4. RESULTS AND DISCUSSION

The Nusselt number data obtained using this method are first compared with the analytical results of Cheng and Minkowycz [1] for isothermal vertical surfaces ($W^* = 0$) to validate the numerical model. As illustrated in Fig. 2, the numerical results correlate well with the analytical results in the higher range of Rayleigh numbers for which boundary layer approximations are valid. However, in the lower range, they begin to diverge. It is apparent that the lower critical limit above which boundary layer type flows are possible can be approximated by a value of $Ra_c \approx 100$ [11]. Below this value, the boundary layer analysis underpredicts the heat transfer rate. At low Rayleigh numbers, diffusion in both directions contributes to the total heat transport. Because the similarity analysis neglects diffusion in the gravitational direction it may underpredict the heat transfer rate.

For the case of higher Ra ($\geq 10^3$), the length of the horizontal impermeable adiabatic surface was varied between 5 and 40% of the height of the vertical surface. The latter limit is twice the estimated boundary layer thickness at $X = 1$. This yields a dimensionless length range of $0.05 \leq W^* \leq 0.4$.

In Fig. 3, the reduced Nusselt number, Nu/Nu_0 is plotted with the dimensionless length, W^*, where Nu_0 is the Nusselt number for $W^* = 0$. As illustrated, even a small flat protrusion at the leading edge produces a drop of approximately 5% in the Nusselt number. As W^* is increased, further reductions in the heat transfer rate occur until a constant reduction of approximately 8% in Nu is attained at a value of approximately $W^* = 0.3$. Further increases in W^* do not appear to affect the heat transfer rates from the vertical surface.

The phenomenon is best explained by referring to the entrainment characteristics of the vertical boundary layer ($W^* = 0$) which entrains mass from the bottom and the side. When a horizontal surface is attached at the leading edge, the entrainment from the bottom is either partially or fully blocked depending on the extent of the horizontal surface W^*.

Figure 4 illustrates typical streamfunction contours ($W^* = 0.2$). The vertical boundary layer thickness at $X = 1$ is approximately the same as the length of the horizontal adiabatic surface at $X = 0$. Entrainment for the vertical boundary layer is supplied primarily from the side and partially from the bottom. As the length of the horizontal side is increased, the source of entrainment shifts entirely, first to the side and then to the top. However, the change in entrainment characteristics influences the heat transfer rate from the wall only when W^* is of the same order of magnitude as the maximum vertical boundary layer thickness. To illustrate this point, the local temperature gradients on the wall are plotted for different values of W^* in Fig. 5. Note that the temperature gradients are identical for $W^* \geq 0.35$. It is also apparent that the wall temperature gradients change with increasing W^* only in the lower 30% of the length of the vertical surface. The vertical velocity profiles at $X = 1$ (not shown) do not change much with W^*, thus the effect of

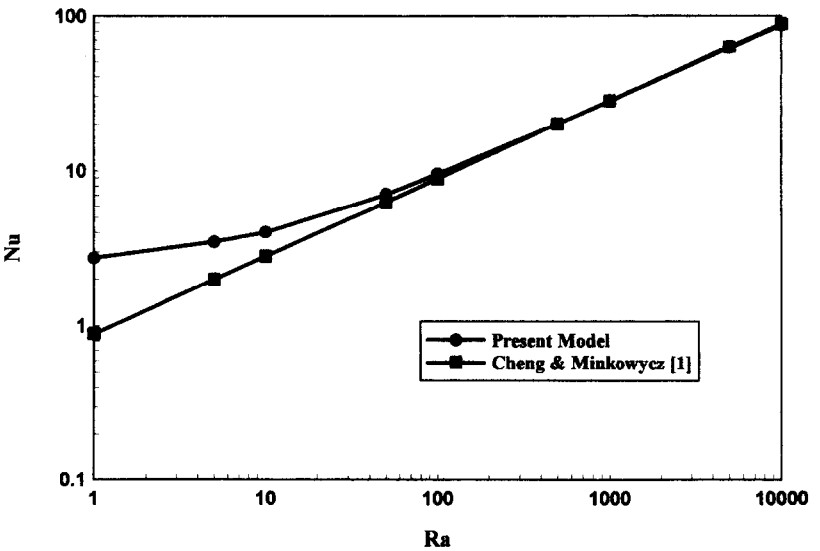

Fig. 2. Comparison of the computed average Nusselt number for a lone vertical surface ($W^* = 0$) with the analytical solution of Cheng and Minkowycz [1].

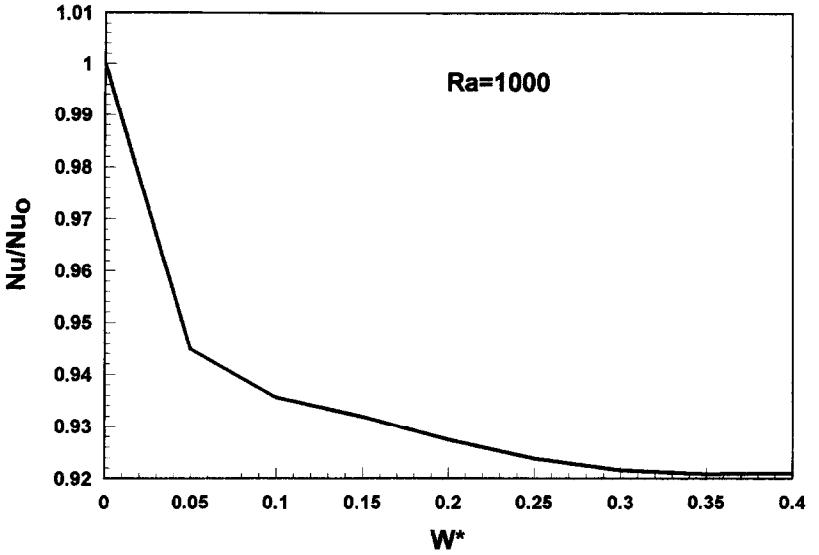

Fig. 3. The variation of the reduced Nusselt number with the length of the horizontal adiabatic extension.

the horizontal side is confined only to the corner region for higher Rayleigh numbers. The entrainment characteristics, however, change significantly as explained above.

As illustrated in Fig. 3, the Nusselt number ceases to change with increasing W^* beyond a certain value which is larger than the vertical boundary layer thickness at $X = 1$. For $Ra = 10^3$, this value of W^* is approximately 0.3 (Fig 3) compared to the estimate of maximum vertical boundary layer thickness given by 0.2. The present study for the corner and the similarity analysis of Cheng and Minkowycz [1] yield

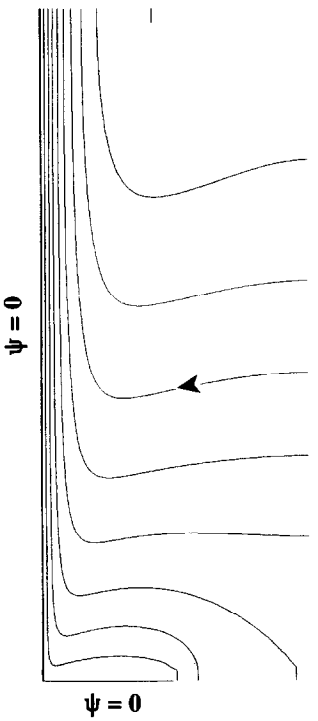

Fig. 4. Streamfunction contours for $W^* = 0.2$ and $Ra = 10^3$. $\Delta\Psi = 0.5 \times 10^{-2}$.

similar results. From this it can be concluded that for a given Rayleigh number, the heat transfer rate from the vertical surface calculated for $W^* = 2\delta^*_L$ will be identical to those for much larger values of W^*. Numerical calculations have been carried out for Rayleigh numbers in the range of $1 \leqslant Ra \leqslant 10^4$ for corners with $W^* = 2\delta^*_L$.

The boundary layer behavior is well-established near the vertical surface for large Rayleigh numbers. The wall-temperature gradients are shallower when compared to those of a lone vertical surface because of the presence of the horizontal adiabatic surface. Here fluid is entrained into the vertical boundary layer from the side and the top; however, if W^* is increased to a very large value, the source of entrainment will shift entirely to the top with no change in the heat transfer and the boundary layer characteristics near the vertical surface [8]. Vertical velocity profiles at $X = 1$ are shown for different Rayleigh numbers in Fig. 6. The boundary layer thickness increases with decreasing Rayleigh number.

It is interesting to note that the thickness in each case is quite close to the value predicted by the similar analysis of Cheng and Minkowycz [1]. The numerical results suggest that the boundary layer analysis is valid at higher Rayleigh numbers away from the corner region, but near the corner region the boundary layer approximations fail for all Rayleigh numbers.

Extensive calculations were done for large, dimensionless lengths, W^* $(=2\delta^*_L)$, for horizontal surface temperatures held at $T = 0$ (ambient temperature). The Rayleigh number range covered is $10^0 \leqslant Ra \leqslant 10^4$. The flow patterns are qualitatively similar to those for the adiabatic horizontal wall. The temperature gradients near the corner are sharper because the horizontal surface gains heat. Consequently, the heat transfer rates are larger when compared to the case with an adiabatic horizontal surface.

Computed Nusselt number data for the vertical surface of the corner with a large horizontal surface were correlated using a least-square fit [10] of the form $Nu = mRa^n$. The results are summarized in Table 1 along with the analytical correlation for a single vertical surface given by Cheng and Minkowycz [1]. No attempt is made here to include the lower Rayleigh number range in the same fit because the deviation of actual values from the fit will be large, thus introducing a large error in the other Nu estimates. It is apparent from these correlations, that for vertical boundary layer type flows in porous media the relationship $Nu \sim Ra^{1/2}$ is valid.

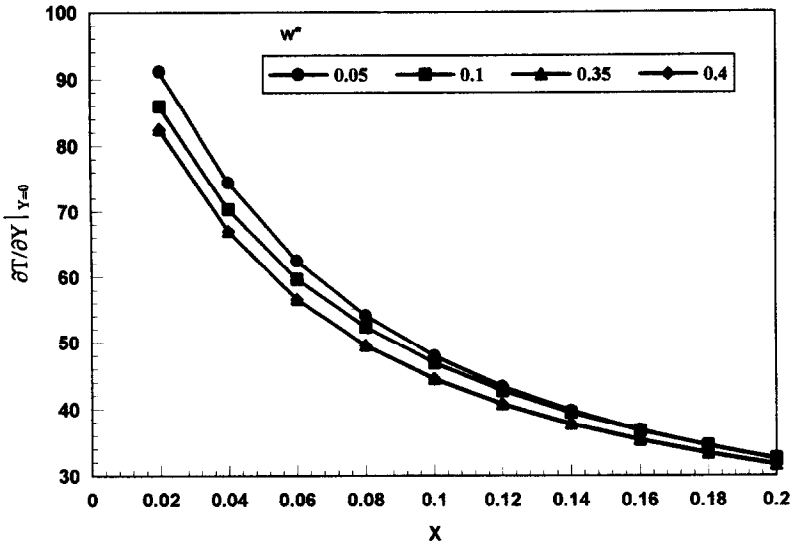

Fig. 5. Local wall temperature gradients for $Ra = 10^3$.

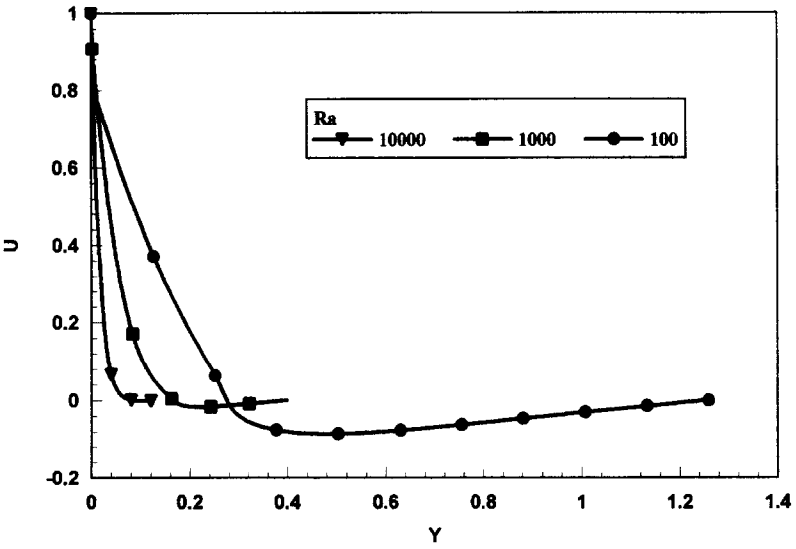

Fig. 6. Vertical velocity profiles at $X = 1$ for 'large' adiabatic W^*.

Table 1. Nusselt number correlations. $Nu = m\,Ra^n$

	Range	m	n
L-shaped corner with adiabatic horizontal (present–numerical)	$W^* > 2\delta_L^*$, $Ra > 100$	0.735	0.51
L-shaped corner with cold isothermal horizontal (present–numerical)	$W^* > 2\delta_L^*$, $Ra > 100$	0.804	0.51
Lone vertical surface (Cheng and Minkowycz [1]–analytical)		0.888	0.5

REFERENCES

1. P. Cheng and W. J. Minkowycz, Free convection about a vertical flat plate embedded in a porous medium with application to heat transfer from a dike, *J. Geophys. Res.* **82,** 2040–2044 (1977).
2. D. A. Nield and A. Bejan, *Convection in Porous Media.* Springer, New York (1992).
3. P. G. Daniels and P. G. Simpkins, The flow induced by a heated vertical wall in a porous medium, *Q. J. Mech. Appl. Math.* **37,** 339–354 (1984).
4. C. T. Hsu and P. Cheng, Effects of upstream geometry on natural convection of a Darcian fluid about a semi-infinite inclined heated surface, *J. Heat Transfer* **107,** 283–292 (1985).
5. Y. Liu and K. A. R. Ismail, Asymptotic solution of free

convection near a corner of two vertical porous plates embedded in porous medium, *Lett. Heat Mass Transfer* **7**, 457–463 (1980).
6. Y. Liu and A. C. Guerra, Free convection in a porous medium near the corner of arbitrary angle formed by two vertical plates, *Int. Commun. Heat Mass Transfer* **12**, 431–440 (1985).
7. Y. Liu, C. Y. Lam and A. C. Guerra, Free convection near a corner formed by two vertical plates embedded in porous medium, *Int. Commun. Heat Mass Transfer* **14**, 125–136 (1987).
8. D. Angirasa and R. L. Mahajan, Natural convection from L-shaped corners with adiabatic and cold isothermal horizontal walls *J. Heat Transfer* **115**, 149–157 (1993).
9. P. J. Roache, *Computational Fluid Dynamics* (Rev. Edn). Hermosa, Albuquerque, NM (1982).
10. W. H. Press, B. P. Flannery, S. A. Teukolsky and W. T. Vetterling, *Numerical Recipes*. Cambridge University Press, New York (1986).
11. P. Cheng and C. T. Hsu, Higher-order approximations for Darcian free convective flow about a semi-infinite vertical flat plate. *J. Heat Transfer* **106**, 143–151 (1984).

Pergamon

Int. J. Heat Mass Transfer. Vol. 40, No. 2, pp. 490–492, 1997

0017–9310/97 $15.00+0.00

PII: S0017–9310(96)00093–2

Symbolic mathematics for the calculation of thermal efficiencies and tip temperatures in annular fins of uniform thickness

ANTONIO CAMPO and R. EUGENE STUFFLE
College of Engineering, Idaho State University, Pocatello, ID 83209, U.S.A.

(*Received* 1 *November* 1995 *and in final form* 29 *February* 1996)

INTRODUCTION

The first heat transfer analyses of fins with different shapes date back to the pioneering contributions of Harper and Brown [1] and Gardner [2], who led the way to numerous research papers on this topic throughout the subsequent years.

Independent of the shape of the fin, the need to estimate the tip temperature as a function of geometric, flow and thermal parameters stems from the fact that these local temperatures have to be within certain bounds to ensure the safety of technical personnel in plant environments (see Muir *et al.* [3]).

Straight fins of uniform thickness are characterized by two dimensions only, length and thickness. Calculation of the heat transfer and the tip temperature of these fins is rather simple, because it requires the evaluation of a hyperbolic tangent and a hyperbolic cosine, respectively. Unfortunately, other fin configurations of equal importance, such as the annular fin of uniform thickness, are characterized by three dimensions, length, thickness and radii ratio. Additionally, the expressions for the heat transfer and the tip temperature involve the evaluation of Bessel functions. These aspects were cleverly circumvented by Gardner [2] who devised a graphical representation of the heat transfer, constructing the so-called fin efficiency diagram. This diagram contained the fin efficiency in the ordinate and a dimensionless thermogeometric parameter as the abscissa. The family of curves was parameterized by the radii ratio, whose range typically goes from 1 up to 5, inclusive. As expected, whenever the radii ratio is not an integer number, the reading in the fin efficiency diagram necessitates 'visual interpolation'. It should be remembered that in those days engineers performed calculations with slide rules. Unequivocally, the above-described computational procedure is incompatible with modern computer aided design (CAD) of annular fins of uniform thickness.

On the other hand, Gardner [2] left untouched an easy parallel procedure linked to the calculation of the corresponding tip temperatures of annular fins of uniform thickness. These calculations could have provided a companion tip temperature diagram to the fin efficiency diagram.

In order to alleviate the minor deficiencies pertinent to the analysis and design of annular fins of uniform thickness, this technical note presents a simple and versatile way that facilitates the rapid determination of both quantities: the fin efficiencies and the tip temperatures, both in terms of the controlling parameters. These calculations have been accomplished with the help of symbolic computational mathematics and the computed results have been post-processed, analyzed and reported in terms of correlation equations of compact form.

MATHEMATICAL ANALYSIS

Consider the steady-state heat transfer in an annular fin of uniform thickness $2t$ in which the inner and outer radius are r_1 and r_2, respectively. For a situation of constant physical properties of the material and negligible heat loss through the tip, the temperature distribution, $\theta(z)$, can be taken from the textbook by Mills [4]

$$\theta(z)=\frac{K_1(z_2)I_0(z)+I_1(z_2)K_0(z)}{I_0(z_1)K_1(z_2)+I_1(z_2)K_0(z_1)}. \qquad (1)$$